


Article

# Integer and Fractional Floquet Resonances in a Driven Three-Well System

Liping Li <sup>1,\*</sup>, Bo Wang <sup>1</sup> and Weibin Li <sup>2,\*</sup> 

<sup>1</sup> Zhengzhou Key Laboratory of Low-Dimensional Quantum Materials and Devices, College of Science, Zhongyuan University of Technology, Zhengzhou 450007, China; 9772@zut.edu.cn

<sup>2</sup> School of Physics and Astronomy, Centre for the Mathematics and Theoretical Physics of Quantum Non-Equilibrium Systems, University of Nottingham, Nottingham NG7 2RD, UK

\* Correspondence: 6716@zut.edu.cn (L.L.); weibin.li@nottingham.ac.uk (W.L.)

**Abstract:** We investigate Floquet dynamics of a particle held in a three-well system driven by a two-frequency field and identify integer and fractional photon resonances due to the dual-frequency driving. It is found that pairs of photon-assisted tunneling near the resonance originate from avoided level crossings in the Floquet spectra which, in essence, are quantum features of the hybridization between different quantum states. In particular, we establish a close connection between fractional-order resonances and Floquet mode properties under two-frequency driving conditions and illustrate their dependence on driving parameters. These results provide us a possibility to realize coherent control of quantum states with the assistance of classical external driving fields.

**Keywords:** dual-frequency driving; Floquet resonance; photon-assisted tunneling



**Citation:** Li, L.; Wang, B.; Li, W. Integer and Fractional Floquet Resonances in a Driven Three-Well System. *Photonics* **2021**, *9*, 738. <https://doi.org/10.3390/photonics9100738>

Received: 10 August 2022

Accepted: 30 September 2022

Published: 8 October 2022

**Publisher's Note:** MDPI stays neutral with regard to jurisdictional claims in published maps and institutional affiliations.



**Copyright:** © 2020 by the authors. Licensee MDPI, Basel, Switzerland. This article is an open access article distributed under the terms and conditions of the Creative Commons Attribution (CC BY) license (<https://creativecommons.org/licenses/by/4.0/>).

## 1. Introduction

Floquet resonance in a periodically driven field is of fundamental importance in quantum control and manipulation in which periodic driving [1–4] has emerged as a technique to realize different applications, for instance, in population trapping [5], quantum phase transition [6,7], atomic transportation [8,9] and quantum information processing [10,11]. Among various models, the paradigmatic two-level and three-level systems, e.g., Rydberg-excited atoms [12], Bose-Einstein condensate (BEC) [13–15], coupled waveguide arrays [16,17] and Dirac electrons [18], have been intensively investigated and exhibit interesting effects including dynamical localization [19], coherent destruction of tunneling (CDT) [20,21] and photo-assisted tunneling (PAT) [22]. Recently, dynamics of monolayer graphene in a time-periodic potential are widely studied in the framework of the Floquet approach and exhibit a number of novel quantum effects [23] such as photon-induced tunneling of electrons [24], chiral tunneling [25], Floquet scattering [26] and voltage-driven quantum oscillations [27]. These findings and approaches that are related to Floquet dynamics open the possibility of controlling quantum states in multiple nanotechnological applications.

In particular, recent numerical algorithms and experimental conditions have developed driving schemes from monochromatic [28] to bichromatic [29], three-frequency [30] and even random-frequency driving models [31], and consequently provide more intriguing results such as multiphoton resonance and fractional photon-assisted tunneling [32]. Esmann and coworkers [33] have revealed that 1/2-photon, 1/3-photon, and 1/4-photon resonances can have large effects on the particle transfer. Strictly speaking, there is no true photon absorption in a driven system and the *photons* are provided by the external driving field. In this paper, resonances corresponding to integer or fractional multiples of a driving frequency are still called photon resonances, which in essence are analogous to those in solids. These extensions of photon resonance in a periodically driven system are of significance and provide a more flexible way to realize how such effects could be applied. For instance, an analog of photon-assisted tunneling [34] is achieved in a coupled optical

waveguide system by only modulating one waveguide and adjusting the distance between two adjacent ones, which may offer benefits for controlling light propagation and realizing all-optical switches.

For these periodically driven systems, Floquet theory provides a useful tool to understand the physical mechanism of some new quantum effects derived from the time-dependent Schrödinger equations (TDSE) [35,36] with a time-periodic Hamiltonian  $H(t) = H(t + T)$  where  $T = 2\pi/\omega$  is the period of external driving fields for all time  $t$ . Recently, Floquet approaches have developed into many types such as Shirley's formulation of Floquet theory (SFT) [37], many-mode Floquet theory (MMFT) [38–40] and instantaneous Floquet state (IFS) [41]. In special cases of multiple periodic fields with commensurate frequencies (integer multiples of a common frequency), Poertner and Martin [42] have proved the equivalence of SFT and MMFT.

These powerful approaches enable us to qualitatively understand Floquet resonances in multiple frequency driving conditions. In this paper, we focus on the peculiar behaviors of tunneling probability at and beyond the resonance by investigating a particle in a three-well lattice subjected to a dc field plus two ac fields. We propose that through driving-induced resonances, one can engineer the parameter space involving six relevant driving parameters for both coherent tunneling and complete population trapping. Also, the ratio between driving amplitude and frequency plays a vital role in exploring features of tunneling dynamics. Our results further demonstrate that pairs of avoided crossings of quasienergies account for the photon-assisted tunneling which is closely related to the symmetrical and anti-symmetrical states. Furthermore, in two-frequency driving conditions, we find that integer and fractional photon-assisted tunneling show obvious dependence on driving amplitudes and phase differences, which provides us with a way to coherently control the tunneling probability between different quantum states.

The rest of this paper is structured as follows. In Section 2, we present the physical model, Floquet theory and SFT method and then introduce a useful transformation in the high-frequency approximation. To characterize the particle's evolution behaviors, we define a physical quantity, namely the tunneling probability, to directly describe the tunneling rate. In Section 3, we revisit integer multiple photon resonances and their physical mechanisms under monochromatic cases. Floquet-based interpretations reveal that pairs of avoided crossings of quasienergies account for photon-assisted tunneling. In Section 4, we indulge in the two-frequency driving cases and find that fractional-order resonances being a large effect on tunneling dynamics can have an excellent explanation by utilizing the Floquet theory under certain conditions. Then, we further analyze dynamic dependences on driving amplitude and phase difference and establish a close connection with Floquet properties. Finally, we summarize our results in Section 5.

## 2. Model and Method

We study a particle confined in a driven system consisting of a linear arrangement of three quantum wells, in which the left-most well (well-1) is driven by a dual-frequency field and the other two wells denoted by  $j$  ( $j = 2, 3$ ) are undriven. Such a three-well (state) model illustrated in Figure 1a can be realized by subjecting ultracold neutral atoms to spatially periodic light-shift potentials arising in the interference patterns of multiple laser beams [43,44]. In particular, Frederik et al. [45] proposed a two-frequency driving case by modulating the position of an optical lattice at two frequencies simultaneously. These experimental results establish the possibility of artificially generating two-frequency driving quantum potentials in an optical lattice. Alternatively, a three-engineered-waveguide system can provide an ideal platform to investigate such driving-induced phenomena by mapping the temporal evolution of quantum dynamics into spatial propagation of light waves. Experimentally, the technology of fs laser written waveguide arrays (see Ref. [46] for full details of the fabrication method) permits our specific setting of the two-frequency driving properties of the waveguides. S. Longhi et al. have provided several methods to realize the selective harmonic modulations by periodically bending

particular waveguides [2,47,48] or by harmonically modulating the refractive index of partial waveguides while keeping the rest fixed [49]. As in the experiments [46], in Figure 1b, we set the top boundary waveguide to have a different refractive index profile compared to the rest waveguides. The width of the individual waveguides is set to be 3 μm and the adjacent waveguide spacing amounts to 32 μm. The input power of light intensity is on the order of MW. Thus, selectively irradiating the top waveguide with two harmonic frequencies is well within the reach of the related experimental setup.

Dynamics of the system is governed by the dimensionless Hamiltonian ( $\hbar = 1$ ) [50–52],

$$H(t) = \varepsilon(t)|1\rangle\langle 1| + g(|1\rangle\langle 2| + |2\rangle\langle 1| + |2\rangle\langle 3| + |3\rangle\langle 2|) \tag{1}$$

where  $|1\rangle, |2\rangle, |3\rangle$  represent the localized state in the three wells correspondingly. Here, the dual-frequency field  $\varepsilon(t) = \Delta + A_1\cos(\omega_1 t) + A_2\cos(\omega_2 t + \phi)$  acts on well-1 with  $\Delta$  being the dc field, and  $A_1, A_2, \omega_1$  and  $\omega_2$  being the driving amplitudes and frequencies of the external driving ac field-1 and field-2 with a phase difference  $\phi$ . The six driving parameters can be tuned to explore the driving-induced photon resonances.  $g$  is the coupling intensity between adjacent wells and couplings between next-nearest-neighbor wells have been neglected. As in the Ref. [53], all the parameters  $\Delta, A_1, \omega_1, A_2$  and  $\omega_2$  are normalized in units of a reference frequency  $\omega_0$  on the order of  $10^2 \text{ s}^{-1}$ , and time  $t$  is normalized in units of  $\omega_0^{-1}$ . Dynamics of this system can be obtained by numerically solving the TDSE  $i\partial/\partial t|\Psi(t)\rangle = H(t)|\Psi(t)\rangle$ , where the quantum state  $|\Psi(t)\rangle = a_1(t)|1\rangle + a_2(t)|2\rangle + a_3(t)|3\rangle$  is expanded with the localized state. Here  $a_j(t)$  represents the probability amplitude at the  $j$ th well and satisfies normalization condition  $|a_1(t)|^2 + |a_2(t)|^2 + |a_3(t)|^2 = 1$ . We will use the population probability  $P_j(t) = |a_j(t)|^2$  to characterize the dynamics.

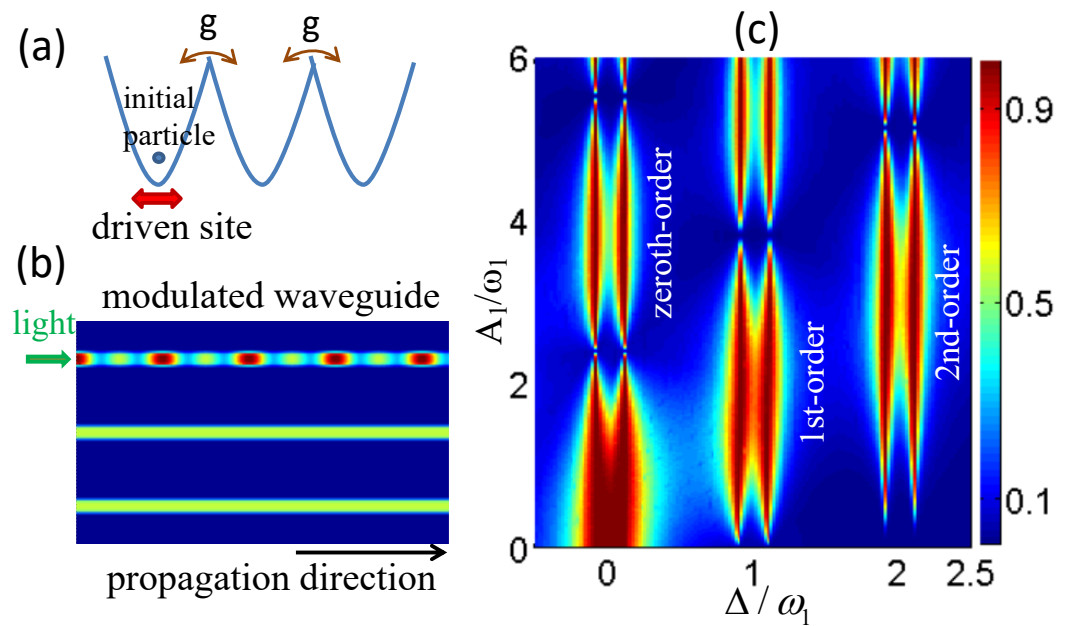


**Figure 1.** (Color online) (a) Schematic diagram for a driven three-well system in which the left-most well (well-1) is driven by a dual-frequency field and the other two wells are undriven. (b) Three-coupled waveguides with selective modulation of the top waveguide (waveguide-1) by two harmonic frequencies. (c) Tunneling probability  $\Pi_1$  as a function of  $\Delta/\omega_1$  and  $A_1/\omega_1$ . Pairs of bright colors are along the  $\Delta/\omega_1$  axis in the vicinity of a series of resonance points  $\Delta/\omega_1 = n$  where  $n$  is an integer. Along the  $A_1/\omega_1$  axis,  $n$ -photon-assisted tunneling is almost completely suppressed ( $\Pi_1 \approx 0$ ) under the conditions of  $J_{-n}(A_1/\omega_1) = 0$ . Parameters are varied by changing  $\Delta$  and  $A_1$  and fixing  $\omega_1 = 10$ . The initial conditions are  $a_1(0) = 1, a_2(0) = 0, a_3(0) = 0$ .

### 2.1. Floquet Theory and SFT Method

When two driving frequencies are rational, i.e.,  $\omega_2/\omega_1 = N_2/N_1$  with  $N_1$  and  $N_2$  being integers, Hamiltonian (1) is periodic in time  $t$  with a common frequency  $\omega = \omega_2/N_2 = \omega_1/N_1$ . According to the Floquet theory [35,36], for a Hamiltonian that is both periodic and hermitian, one could write three independent solutions for quantum state  $|\Psi(t)\rangle$  of the form,

$$|\Psi_j(t)\rangle = e^{-iE_j t} |\phi_j(t)\rangle \tag{2}$$

where we have labeled each solution with index  $j$ .  $E_j$  and  $|\phi_j(t)\rangle$  are the quasienergies and corresponding Floquet states with a same periodicity as the Hamiltonian,  $|\phi_j(t)\rangle = |\phi_j(t + T)\rangle$ . Hence we find  $|\Psi_j(t + T)\rangle = |\Psi_j(t)\rangle e^{-iE_j T}$  and the unitarity of  $|\Psi(t)\rangle$  at all times guarantees that diagonal elements  $E_j$  of quasienergies are real.

Since Hamiltonian (1) is also hermitian, we can define a unitary time evolution operator,  $U(t, 0)$ , satisfying,

$$|\Psi(t)\rangle = U(t, 0) |\Psi(0)\rangle \tag{3}$$

for all time  $t$ . Here, we have assumed that the initial time for evolution is given at  $t_0 = 0$ . From the equation of TDSE, one can find that  $U(T, 0) = \mathcal{T} e^{-i \int_0^T H(t) dt}$  where  $\mathcal{T}$  denotes the time-ordering operator. Then, for the unitary case [53], the operator  $U(t, 0)$  is obtained formally,

$$U(t, 0) = \sum_j |\phi_j(t)\rangle e^{-iE_j t} \langle \phi_j(0) | \tag{4}$$

Therefore, the quasienergies and quasistates of Equation (2) can be obtained by numerically solving the time evolution operator over one period of the driving.

Based on Floquet’s theorem, Shirley [37,42] provides an alternative to direct integration, namely the SFT method, which relates the semiclassical time-dependent Hamiltonian to a time-independent Hamiltonian represented by an infinite matrix. In the following, we present briefly the SFT method in the case of a single frequency field. It can be extended to multiple frequencies [37,42]. However, we find the method is more convenient in dealing with single frequency fields as insights revealed by the method. Due to the periodicity of  $|\phi_j(t)\rangle$ , one can apply the SFT method through Fourier decomposition of the Floquet states,

$$|\phi_j(t)\rangle = \sum_n e^{in\omega t} |\tilde{\phi}_j(n)\rangle \tag{5}$$

where  $\omega = 2\pi/T$  and  $n$  to be an integer. Here we have defined SFT Floquet state  $|\tilde{\phi}_j(n)\rangle = |\tilde{\phi}_j\rangle \otimes |n\rangle$ , where  $\{|n\rangle\}$  denotes the modes of the driving fields and forms an orthonormal basis. Note that Equation (2) can also be written as  $|\Psi_j(t)\rangle = \sum_n e^{-i(E_j - n\omega)t} |\tilde{\phi}_j(n)\rangle$ . Therefore, the SFT method is considered as the famous replicas of Floquet states, and their quasienergies are given by,

$$E_{j,n} = E_j - n\omega \tag{6}$$

Because the periodic Hamiltonian (1) can also be expanded as  $H(t) = \sum_m \tilde{H}(m) e^{im\omega t}$  where  $m$  is also an integer, the TDSE can be expressed in terms of the  $|\tilde{\phi}_j(n)\rangle$  and  $\tilde{H}(m)$  and expansion coefficients are determined from a time-independent matrix (the Floquet Hamiltonian). In our system, each  $\tilde{H}(m)$  is a  $3 \times 3$  matrix. The coupled time-independent equation is,

$$\sum_{j,n} H_F |\tilde{\phi}_j(n)\rangle = \sum_{j,n} E_j |\tilde{\phi}_j(n)\rangle \tag{7}$$

where  $j$  runs over all the atomic states before each change in  $n$ . This result is a linear eigenvalue problem and the Floquet Hamiltonian  $H_F$  can be conveniently defined by Dirac notation [37],

$$\langle im|H_F|jn\rangle = \tilde{H}_{ij}(m - n) + m\omega\delta_{ij}\delta_{mn} \tag{8}$$

where the index  $i(j)$  represents an atomic state, but the index  $m(n)$  represents a Fourier component. We can see that the Floquet Hamiltonian has a periodic structure with multiple  $\omega$  in the diagonal elements. Based on this SFT method, Floquet quasienergies and Floquet states are determined by an infinity time-independent matrix  $H_F$  which is solvable by appropriately truncating the standard basis for the Fourier space. Instead of summation over all integer  $m$ , here we only consider a finite set  $\{m_{min} \leq m \leq m_{max}\}$  and for the validity and simplicity, we select  $m_{max} = -m_{min}$ . Then as Poertner and Martin have pointed out in Ref. [42], the truncated Fourier series  $m_{max} \geq 10$  is necessary to compute Equation (7).

### 2.2. High-Frequency Approximation

As an effective analytical method, a high-frequency approximation is required to obtain approximate analytical solutions to the governing equation as analytical results can provide a better intuitive understanding of the physics. High-frequency approximation arises when the driving frequency exceeds other characteristic frequencies of the system [54–58]. In that case, one can construct a high-frequency expansion of an effective time-independent Hamiltonian of the system by averaging out the high-frequency terms. In this paper, it is found that the high-frequency limit works well under the condition of  $\omega \geq 10g$ . We first apply the high-frequency approximation to gain some insight into the tunneling dynamics. By introducing the transformation  $a_1(t) = b_1(t)e^{-i \int \epsilon(t)dt}$ ,  $a_2(t) = b_2(t)$ ,  $a_3(t) = b_3(t)$ , we use the slowly varying function of time  $b_j(t)$  to describe the evolution of tunneling dynamics and then obtain a coupled equation,

$$\begin{aligned} i\frac{db_1(t)}{dt} &= ge^{i \int \epsilon(t)dt}b_2(t) \\ i\frac{db_2(t)}{dt} &= ge^{-i \int \epsilon(t)dt}b_1(t) + gb_3(t) \\ i\frac{db_3(t)}{dt} &= gb_2(t) \end{aligned} \tag{9}$$

where the terms  $ge^{\pm i \int \epsilon(t)dt}$  describe the coupling between the driven well-1 and undriven well-2, which is effectively modified by six driving parameters. After further using the Jacobi-Anger expansion  $e^{\pm ix\sin\theta} = \sum_{n'=-\infty}^{\infty} J_{n'}(x)e^{\pm in'\theta}$  with  $J_{n'}(x)$  being the  $n'$ th-order ordinary Bessel function of  $x$ , we can get the expansion  $e^{\pm i \int \epsilon(t)dt} = e^{\pm i[\Delta t + \frac{A_1}{\omega_1}\sin(\omega_1 t) + \frac{A_2}{\omega_2}\sin(\omega_2 t + \phi)]} = \sum_{n_1} \sum_{n_2} J_{n_1}(\frac{A_1}{\omega_1})J_{n_2}(\frac{A_2}{\omega_2})e^{\pm i[(\Delta + n_1\omega_1 + n_2\omega_2)t + n_2\phi]}$  where  $n'$ ,  $n_1$  and  $n_2$  are integers. In the high-frequency approximation, the higher-order terms which are proportional to  $\propto e^{\pm in_1\omega_1 t}$  and  $\propto e^{\pm in_2\omega_2 t}$  where  $n_1, n_2 \geq 1$  vary rapidly and their average over a time scale larger than  $\omega_l^{-1}$  ( $l = 1, 2$ ) is zero. These terms can therefore be neglected. Hence we could obtain some analytical solutions which display fascinating physical phenomena such as dynamical stabilization and multiple photon resonances. For instance, when  $\Delta = A_2 = 0$ , our model is identical to that of the periodically driven three-level system by a monochromatic field [59,60]. In the high-frequency regime,  $e^{\pm i \int \epsilon(t)dt} \approx J_0(\frac{A_1}{\omega_1})$ , the effective coupling between well-1 and well-2 is  $g_{eff} = gJ_0(\frac{A_1}{\omega_1})$ . The CDT effect occurs at a series of isolated driving parameter points which satisfy  $J_0(\frac{A_1}{\omega_1}) = 0$  [20,21].

To characterize dynamic behaviors, we define the tunneling probability  $\Pi_j$  as,

$$\Pi_j = 1 - \min[P_j(t)] \tag{10}$$

where  $P_j(t) = |a_j(t)|^2 = |b_j(t)|^2$  denotes the population probability of the particle at the  $j$ th well and  $\min[P_j(t)]$  is the minimum value of  $P_j(t)$  within a finite time interval ( $t \in [0, 100]$ ). Under this definition,  $\Pi_j = 1$  means the probability of the particle initially trapped at the  $j$ th well can completely tunnel into other wells, while  $\Pi_j = 0$  indicates the occurrence of population trapping or dynamical localization of the state  $|j\rangle$  in the simulation. Therefore, the value of  $\Pi_j$  allows to directly measure the tunneling rate from state  $|j\rangle$  to other states.

### 3. Integer Photon Resonance with a Single-Frequency Driving Field

In this section, we investigate integer photon resonances with one ac field (i.e.,  $A_2 = 0$ ). In particular, we reveal a close relation between resonance dynamics and Floquet mode properties. To illustrate this relation, we first show dynamical evolution of  $\Pi_1$  versus  $\Delta/\omega_1$  and  $A_1/\omega_1$  in Figure 1c, where we change parameters  $\Delta$  and  $A_1$  and fix  $\omega_1 = 10$ . The initial conditions are  $a_1(0) = 1, a_2(0) = 0, a_3(0) = 0$  and we choose  $g = 1$ . When  $\Delta/\omega_1$  varies from 0 to 2.5, one finds that, in the horizontal direction, three pairs of resonance features are illustrated, and bright colors indicate higher tunneling rates. It is seen that quantum tunneling from well 1 to the other two wells is greatly restored when  $\Delta/\omega_1$  is about an integer. If assuming  $\Delta = n\omega_1 + \delta$  where  $|\delta| \leq \frac{\omega_1}{2}$  and  $n$  being an integer, parameters corresponding to  $n = 0, 1, 2$  where  $\delta = 0$  are usually called resonance points. One can define the tunneling near these points as  $n$ -photon-assisted tunneling, i.e., zeroth-order, 1st-order and 2nd-order PAT as marked in Figure 1c. In the vertical direction, it is seen that the zeroth-order photon-assisted tunneling is almost completely suppressed when  $A_1/\omega_1$  equals to 2.4, and 5.5, satisfying  $J_0(A_1/\omega_1) = 0$ . According to the high-frequency approximation in Equation (9), one can see that the right-hand side of the equation vanishes, which suppresses the tunneling. Similarly, one can find the suppression of other orders. For example, the 1st-order photon-assisted tunneling is inhibited when  $A_1/\omega_1$  equals 3.8 satisfying  $J_{\pm 1}(A_1/\omega_1) = 0$ . Finally, we rewrite Equation (9) in the high-frequency approximation using the Bessel functions,

$$\begin{aligned} i\frac{db_1(t)}{dt} &= gJ_{-n}\left(\frac{A_1}{\omega_1}\right)e^{i\delta t}b_2(t), \\ i\frac{db_2(t)}{dt} &= gJ_{-n}\left(\frac{A_1}{\omega_1}\right)e^{-i\delta t}b_1(t) + gb_3(t), \\ i\frac{db_3(t)}{dt} &= gb_2(t). \end{aligned} \tag{11}$$

Clearly, tunneling probabilities between wells are completely inhibited under the conditions of  $J_{-n}\left(\frac{A_1}{\omega_1}\right) = 0$ , indicating the occurrence of population trapping and the particle will be localized at the initial well.

#### 3.1. Physical Explanation of Photon-Assisted Tunneling

To understand the physical mechanism of integer photon-assisted tunneling, we first investigate the properties of Floquet quasienergies based on the SFT method. Driven by the single-frequency field, the relevant Floquet Hamiltonian has a simple form,

$$\tilde{H}(0) = \begin{pmatrix} \Delta & g & 0 \\ g & 0 & g \\ 0 & g & 0 \end{pmatrix}, \quad \tilde{H}(\pm 1) = \begin{pmatrix} A_1/2 & 0 & 0 \\ 0 & 0 & 0 \\ 0 & 0 & 0 \end{pmatrix}. \tag{12}$$

We can diagonalize  $H_F$  (truncated at  $m_{max} = 20$ ) to obtain the quasienergies for  $A_1 = 22$ . Three replicas are presented in Figure 2a corresponding to  $m = -1, 0, 1$ . The ratio  $\Delta/\omega_1$  is varied by changing  $\Delta$  and fixing  $\omega_1$ . Other parameters are  $\omega_1 = 10$  and  $g = 1$ . Avoided level crossings of the quasienergy are clearly displayed near  $\Delta/\omega_1 = 0, 1, 2, 3$ . The partially enlarged illustration (the insert in Figure 2a) shows that there are no degeneracy points in this quasienergy spectrum. The hybridization between different quantum states around the avoided level crossing leads to photon-assisted tunneling. To confirm this, we

numerically solve the TDSE and plot  $\Pi_1$  as a function of  $\Delta/\omega_1$  for  $A_1 = 22$  in Figure 2b. It is seen that at these avoided crossings, photon-assisted tunneling is identified as pairs of sharp peaks in  $\Pi_1$ .

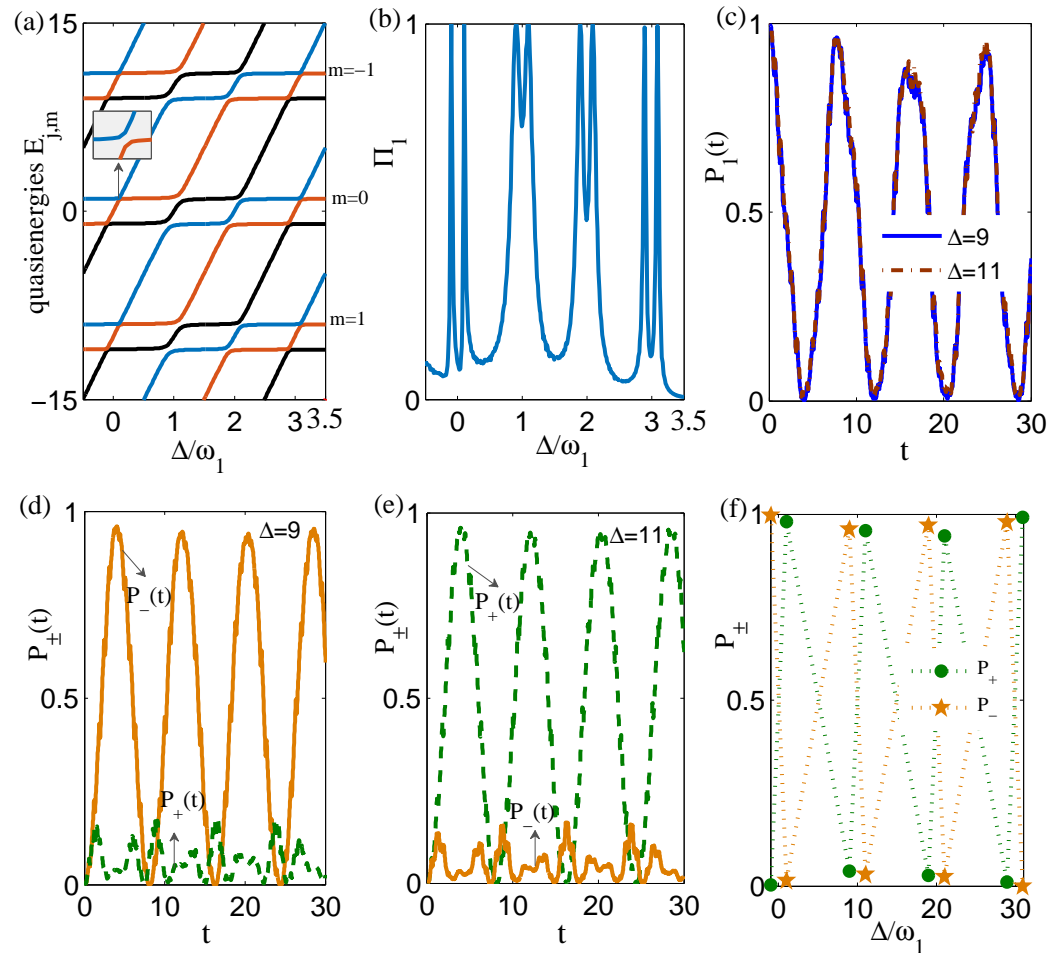


**Figure 2.** (Color online) (a) Floquet quasienergies and (b)  $\Pi_1$  as a function of  $\Delta/\omega_1$  show pairs of avoided crossings and photon-assisted tunneling. (c) Evolution of occupations at well 1  $P_1(t) = |a_1(t)|^2$  for two cases of  $\Delta = 9$  and  $\Delta = 11$ . (d,e) Evolution of occupations at the symmetrical state  $P_+(t)$  and anti-symmetrical state  $P_-(t)$  for (d)  $\Delta = 9$  and (e)  $\Delta = 11$ . (f) Population probabilities  $P_+$  and  $P_-$  corresponds to the avoided crossings. The values are derived when  $P_1$  reaches zero for the first time. The parameters are chosen as  $A_1 = 22$ ,  $\omega_1 = 10$  and  $g = 1$ .

As an important aspect within this analysis, we further identify which states are actually excited at the avoided crossings by looking at the occupation in the basis of  $|1\rangle$ ,  $|+\rangle = \frac{1}{\sqrt{2}}(|2\rangle + |3\rangle)$  and  $|-\rangle = \frac{1}{\sqrt{2}}(|2\rangle - |3\rangle)$ . Evolutions of occupations at well 1  $P_1(t) = |a_1(t)|^2$  for two cases of  $\Delta = 9$  and  $\Delta = 11$  are plotted in Figure 2c. It is seen that evolutions for the 1st-order resonance tunneling under these two conditions keep the same properties. Then occupations at the symmetrical state  $|+\rangle$ , i.e.,  $P_+(t) = |\langle \Psi(t) | + \rangle|^2$  and the anti-symmetrical state  $|-\rangle$ , i.e.,  $P_-(t) = |\langle \Psi(t) | - \rangle|^2$  are displayed in Figure 2d,e. For  $\Delta = 9$ ,  $P_-(t)$  oscillates with a higher amplitude, while  $P_+(t)$  keeps a lower value. However, for  $\Delta = 11$ , we see the opposite. Moreover, occupations at the symmetrical state  $|+\rangle$  and the antisymmetrical state  $|-\rangle$  at four pairs of avoided crossings are carefully checked, as shown in Figure 2f, which demonstrates that when  $P_1(t) = 0$ , the particle tunnels into a hybrid state between well 2 and well 3. These values are numerically derived when  $P_1(t)$  reaches zero for the first time. Therefore, the left tunneling peak at the  $n$ th-order resonance is closely related to the anti-symmetrical state and the right one is associated with the symmetrical

state. In a brief, we attribute pairs of photon-assisted tunneling in Figures 1c and 2b to avoid crossings in the quasienergies which, in essence, are the quantum feature of the hybridization between different quantum states.

### 3.2. Manipulation of Nth-Order Photon-Assisted Tunneling

In this subsection, we focus on the control of tunneling dynamics. From Figure 1c, we learn that n-photon-assisted tunneling will be greatly suppressed once the conditions  $J_{-n}(\frac{A_1}{\omega_1}) = 0$  are satisfied. Inspired by this, we provide a scheme to manipulate the nth-order resonance dynamics. In Figure 3, we show the Floquet spectra and tunneling probabilities  $\Pi_1$  in terms of  $\Delta/\omega_1$  with  $\frac{A_1}{\omega_1} = 2.4$  and  $\frac{A_1}{\omega_1} = 3.8$ . The left column is for  $A_1 = 24, \omega_1 = 10$  satisfying  $J_0(\frac{A_1}{\omega_1}) = 0$ , while the right column is for  $A_1 = 38, \omega_1 = 10$  which is a zero solution of  $J_1(\frac{A_1}{\omega_1}) = 0$ . We find that for  $J_0(\frac{A_1}{\omega_1}) = 0$ , as shown in Figure 3a,b, when quasienergy levels tend to be degenerate near  $\Delta/\omega_1 = 0$ , the zeroth-order tunneling peaks in  $\Pi_1$  are suppressed. Then, for  $J_1(\frac{A_1}{\omega_1}) = 0$ , as shown in Figure 3c,d, the Floquet spectrum becomes almost a crossing point near  $\Delta/\omega_1 = 1$  where 1st-order photon-assisted tunneling is inhibited. Such conclusions can be extended to suppress nth-order photon-assisted tunneling by changing ratio  $\frac{A_1}{\omega_1}$  to satisfy  $J_{-n}(\frac{A_1}{\omega_1}) = 0$ . Analytically, when  $A_1 = 38, \omega_1 = 10$ , the 1st-order photon-assisted tunneling is inhibited where  $P_1 \sim 1$ . For  $\Delta/\omega_1 = 0, 2, 3$ , profiles of  $\Pi_1$  is nearly identical (in Figure 3d) due to  $J_0(3.8) \approx J_{-2}(3.8) \approx J_{-3}(3.8)$ . These results provide an opportunity to control nth-order photon-assisted tunneling by choosing the driving amplitude and frequency.

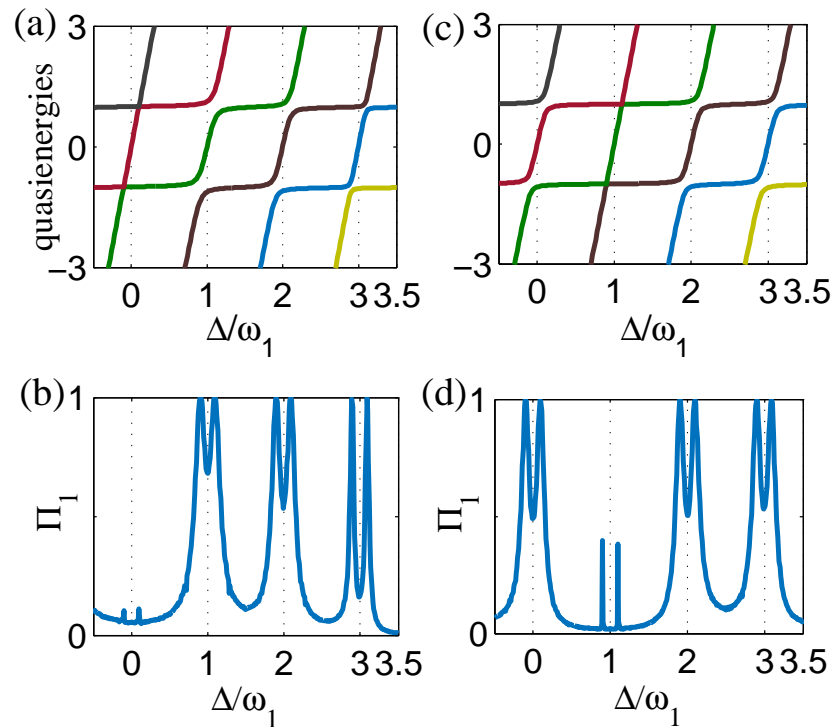


**Figure 3.** (Color online) Floquet quasienergies and evolution of  $\Pi_1$  versus  $\Delta/\omega_1$  with  $\frac{A_1}{\omega_1} = 2.4$  in (a,b) and  $\frac{A_1}{\omega_1} = 3.8$  in (c,d). Other parameters are  $\omega_1 = 10$ , and  $g = 1$ .

### 4. Fractional Floquet Resonance under Two-Frequency Driving

In this section, we investigate fractional photon resonance when the system is driven by a two-frequency field. For concreteness, we set  $\Delta = 0$  such that the driving field becomes a superposition of two simple harmonic driving fields  $\epsilon(t) = A_1 \cos(\omega_1 t) + A_2 \cos(\omega_2 t + \phi)$ . To illustrate the dynamics, we first present numerical results by considering  $A_1 = A_2 = 22$  and  $\phi = 0$ , as shown in Figure 4a, in which pairs of straight lines with bright colors denoting



high tunneling rates (or large  $\Pi_1$ ) are observed at different ratios of  $\nu = \omega_2/\omega_1$ , such as  $\nu = 1, 2, 1/2, \dots$ . These  $\nu$ -photon-assisted tunneling effects come from the applied ac field-2 without which the particle has a very low probability of tunneling into other wells because  $A_1/\omega_1 = 2.2$  belonging to a particular tunneling suppression phenomenon [59]. It is seen that in regions where tunneling should be suppressed, tunneling can be restored when the other drive frequency  $\omega_2$  is an integer multiple or fraction of the drive frequency  $\omega_1$ . In the low-frequency region, tunneling dynamics display a complex resonance pattern, while in the high-frequency region, it tends to have a stable constant value. Compared to the single frequency driving case, the two-frequency driving scheme offers richer dynamics, i.e., leading to both integer and fractional Floquet resonances. Considering the physics of the side with fractional  $\nu$  is just the same as the one with integer  $\nu$  in Figure 4a, we incorporate the fractional transitions like  $\nu = 1/2$  into integer ones like  $\nu = 2$ . In the following, we just investigate in detail the fractional transitions, such as  $\nu = 2/3$ .

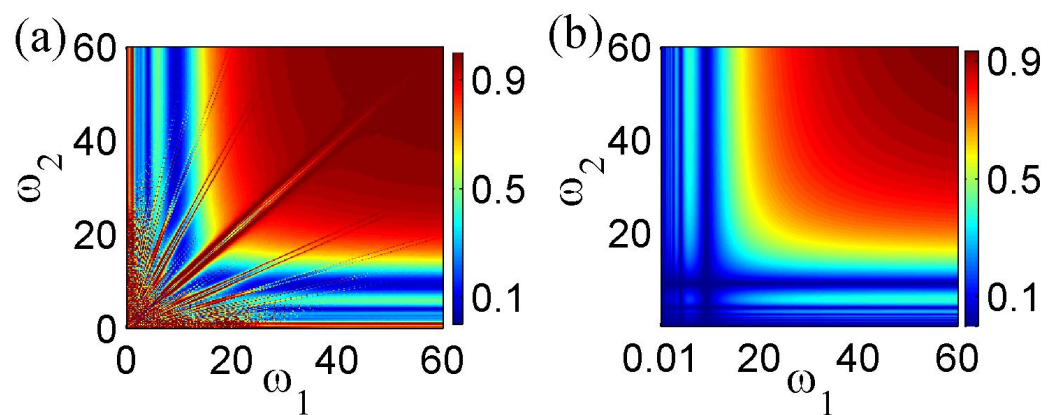


**Figure 4.** (Color online) (a) Numerical results of  $\Pi_1$  and (b) analytical results of coupling intensity  $|g_{eff}|$  as a function of  $\omega_1$  and  $\omega_2$  in the two-frequency driven scheme. Pairs of bright straight lines in (a) denote  $\nu$ -photon-assisted tunneling effects. Analytical results of coupling intensity agrees well with the numerical ones in the high-frequency approximation. Other parameters are chosen as  $A_1 = A_2 = 22, \phi = 0$  and  $g = 1$ .

#### 4.1. Fractional Photon-Assisted Tunneling

To explore the physical mechanism of these resonances, we show  $\Pi_1$  versus  $\omega_2$  in Figure 5a,b for  $A_1 = A_2 = 22$ . Other parameters are  $\omega_1 = 10, g = 1$  and  $\phi = 0$ . When  $\omega_2$  varies in the low-frequency region ( $\omega_2 < 10$ ),  $\Pi_1$  increases to 1 and followed by multiple transitions between coherent tunneling and its suppression. As shown in Figure 5b, the dip positions, from left to right, exactly correspond to the ratios  $\nu = 1/6, 1/5$  and  $1/4$  etc. What's more, values of  $\Pi_1$  are less than 0.5 when  $\nu = 2/3$  and even  $\nu = 3/4$ , suggesting that tunneling suppression at  $\nu$ th-order fractional photon resonances are not trivial effects. In the moderate-frequency region, when  $10 < \omega_2 < 50$ , we note that when  $\omega_2 = 15$ , i.e.,  $\omega_2/\omega_1 = 3/2$ , there exists a pair of fractional photon-assisted tunneling peaks, together with a series of integer-multiphoton-like resonances. As expected, when  $\omega_2$  is in the high-frequency region ( $\omega_2 > 50$ ), the curve ends up with a plateau representing a very low tunneling rate. More simulation results reveal that such resonance effects still exist even if  $A_1 \neq A_2$ , as shown in Figure 5c which is plotted under the condition of  $A_1 = 22$  and  $A_2 = 10$ . Other parameters are the same as in Figure 5a. Then one may wonder whether the integer and fractional resonances appear particularly in driven three-wells. For this reason, we particularly plot the evolution of  $\Pi_1$  versus  $\omega_2$  for the driven two-well system (i.e., by disconnecting the 3rd well) in Figure 5d with the same parameters as in Figure 5a. A series of dips without tunneling peaks (photon-assisted tunneling) is observed and clearly, in such a two-well model, resonance effects manifest as a series of tunneling suppression,

as discussed in Ref. [12]. Therefore, this suggests that the driven three-well system is the simplest model to investigate integer and fractional Floquet resonances.

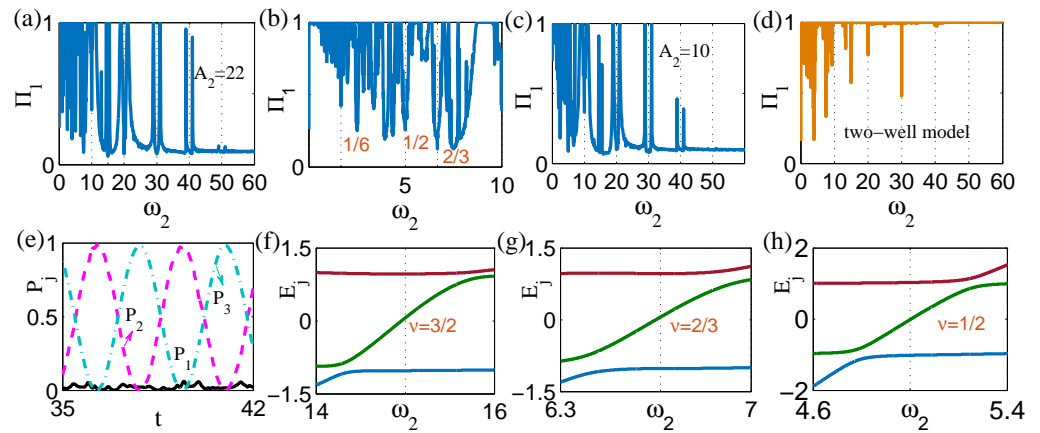


**Figure 5.** (Color online) Plots in the first row represent evolutions of  $\Pi_1$  as a function of  $\omega_2$  for the driven three well system in (a–c) and the driven two well system in (d). (e) Evolution of the probability  $P_j$  at three wells when photon-assisted tunneling occurs. Plots (f–h) are the quasienergies  $E_j$  versus  $\omega_2$  at different fractional resonances which respectively are  $\nu = 3/2, 2/3$  and  $1/2$ . The parameter  $A_2 = 10$  in (c) and  $A_2 = 22$  in other plots. Other parameters are chosen as  $\omega_1 = 10, A_1 = 22, g = 1, \phi = 0$  and time  $t$  is within 100 time units.

To find out where the particle is when fractional photon-assisted tunneling occurs, we calculate the population probabilities at well 2 and well 3 when  $P_1 = 0$ . Taking 3/2nd-order PAT as an example, as shown in Figure 5e, when  $P_1$  reaches zero within a short time interval (between 35-time units and 42-time units), we find that the particle oscillates between well 2 and well 3. Thus, pairs of fractional PAT still correspond to the two hybrid states between wells 2 and 3.

As discussed in Section 2, if  $\omega_2/\omega_1$  can be expressed as the ratio of two integers  $\nu = N_2/N_1$ , the Hamiltonian (1) has a common frequency  $\omega = \omega_1/N_1 = \omega_2/N_2$ . However, it is challenging for us to obtain accurate quasienergies for such a condition with two varying frequencies because the common frequency always changes for different  $\nu$ . Considering inconveniences of the SFT method in solving the variable dual-frequency problem, we turn to the basic Floquet theory and choose a finite narrow parameter range around the resonance to obtain some Floquet-based quasienergy spectra by solving the time evolution operator  $U(T, 0)$  over one period of  $T = 2\pi/\omega$ . For example, in the case of  $\nu = 3/2$ , as shown in Figure 5f, we set the common frequency  $\omega = \omega_1/2 = \omega_2/3 = 5$  to calculate the quasienergies when  $\omega_2$  varies between 14 and 16. When  $\nu = 2/3$ , as shown in Figure 5g, the common frequency is  $\omega = \omega_1/3 = \omega_2/2 = 10/3$  and  $\omega_2$  varies from 6.3 to 7. Other parameters are chosen as  $A_1 = A_2 = 22, \phi = 0$  and  $g = 1$ . We find that at the resonance, three quasienergy levels are separated and the tunneling dynamics are inhibited. While near the resonance, pairs of avoided crossings are attributed to the fractional photon-assisted tunneling. Similarly, utilizing this method, we carefully check all the dips and their corresponding quasienergy spectra, as shown in Figure 5h, in which we list another typical case of  $\nu = 1/2$ . Comparing these results, we can have a deeper understanding of the complicated  $\nu$ -photon resonance. For very low values of  $\omega_2$ , the common frequency  $\omega$  must be much lower than  $\omega_1$  and the three quasienergies oscillating in the range  $(-\omega/2, \omega/2)$  tend to be degenerated, leading to high tunneling rates. When two quasienergy levels form the structure of avoided crossing, the particle can transfer from one state to another. Due to the common frequencies, the spectrum has a complicated energy level structure, resulting in complex resonance patterns in the low-frequency region. These numerical results reveal that Floquet theory still works well near the resonance even if the common frequency changes slightly and we can conclude that it is the avoided crossing of

the Floquet quasienergy that brings the occurrence of integer or fractional photon-assisted tunneling.

#### 4.2. Analytical Analysis in the High-Frequency Approximation

To obtain more intuitive explanations, we focus on the analytical analysis in this part. It is observed that when both  $\omega_1 > 20$  and  $\omega_2 > 20$ , as shown in Figure 4a, these parameters fall in the high-frequency region, and the result can be explained analytically with the high-frequency approximation. The coupling intensity between well-1 and well-2  $g_{eff} = g e^{i \int \epsilon(t) dt}$  (see Equation (9)) can be rewritten by assuming  $\omega_2 = n\omega_1 + \sigma$  where  $\sigma \leq \omega_1/2$  as,

$$g_{eff} = g[\dots + J_{-1}(A_2/\omega_2)J_n(A_1/\omega_1)e^{-i\sigma t} + J_0(A_2/\omega_2)J_0(A_1/\omega_1) + J_1(A_2/\omega_2)J_{-n}(A_1/\omega_1)e^{i\sigma t} + \dots] \tag{13}$$

For small values of  $A_1/\omega_1$  and  $A_2/\omega_2$ , the effective coupling is mainly governed by  $gJ_0(\frac{A_1}{\omega_1})J_0(\frac{A_2}{\omega_2})$ . This analytical result of  $|g_{eff}| = g|J_0(\frac{A_1}{\omega_1})J_0(\frac{A_2}{\omega_2})|$ , as shown in Figure 4b, has a good agreement with the numerical ones in Figure 4a in the high frequency ranges. For instance,  $g_{eff}$  tends to  $g = 1$  if both  $\omega_1$  and  $\omega_2$  hold high values, resulting in a higher tunneling rate. However, we haven't found any evidence of fractional photon-assisted tunneling in Figure 4b, which proves that fractional resonance could be a combination of higher-order transitions. The further analytical result of the population amplitude at well-1 is yielded by solving the coupled Equation (9),

$$b_1(t) = \frac{J_0(\frac{A_1}{\omega_1})J_0(\frac{A_2}{\omega_2})\cos(\chi t) + 1}{1 + J_0(\frac{A_1}{\omega_1})^2J_0(\frac{A_2}{\omega_2})^2} \tag{14}$$

where  $\chi = g\sqrt{1 + J_0(\frac{A_1}{\omega_1})^2J_0(\frac{A_2}{\omega_2})^2}$ . If the two driving frequencies are very high,  $|J_0(\frac{A_1}{\omega_1})J_0(\frac{A_2}{\omega_2})|$  tends to be 1, determining the values of population amplitude at well-1 varying between 0 and 1. These analytical predictions agree well with the numerical results.

In addition, we also note that when one driving frequency is fixed,  $\Pi_1$  tends to be a constant value with the increase of another frequency. For instance, when  $\omega_1 = 10$  and  $\omega_2$  is larger than 50, as shown in Figure 5a,  $\Pi_1$  is almost zero, exhibiting the occurrence of coherent population trapping. The higher  $\omega_2$  is, the weaker the influence of  $J_0(A_2/\omega_2)$  on the coupling intensity. Therefore, in the parameter range  $\omega_2 > 50$ ,  $g_{eff} \approx gJ_0(\frac{A_1}{\omega_1})J_0(\frac{A_2}{\omega_2}) \approx gJ_0(\frac{A_1}{\omega_1}) \approx 0.11g$ , we see almost decoupling between well 1 and well 2 in Figure 5a. The analysis shows that the effective coupling intensity plays a critically important role in controlling tunneling.

#### 4.3. Dependence on Driving Amplitudes

Using the 2/3rd-order resonance as an example, we investigate the dependence on the driving amplitude. The evolution of  $\Pi_1$  versus  $A_1$  and  $A_2$  is plotted in Figure 6a with  $\omega_1 = 10$  and  $\omega_2 = 20/3$ . For  $\omega_2/\omega_1 = 2/3$ , the 2/3rd-order photon-assisted tunneling effect becomes significant in the weak-driving parameter region, i.e.,  $A_1$  and  $A_2$  being very small, in which the value of  $\Pi_1$  can reach 1, manifesting that the particle can almost completely tunnel into other wells. This result can be understood because the weak-driving conditions are similar to those in the high-frequency approximation. when  $A_1$  and  $A_2$  are very small, the effective coupling  $g_{eff}$  in Equation (13) may also tend to be  $g$ . Interestingly, we note that the complete tunneling suppression can be observed in a wide parameter range except for some special cases such as  $45 < A_1 < 55$  and  $55 < A_2 < 65$ , in which  $\Pi_1$  oscillates around 0.5, indicating the particle has half the probability to tunnel into other states. More simulations show that when the condition of  $\omega_2/\omega_1$  changes, the dependence

of tunneling dynamics on driving amplitudes will be different and these results provide us a scheme to enter or exist  $\nu$ -photon resonance.

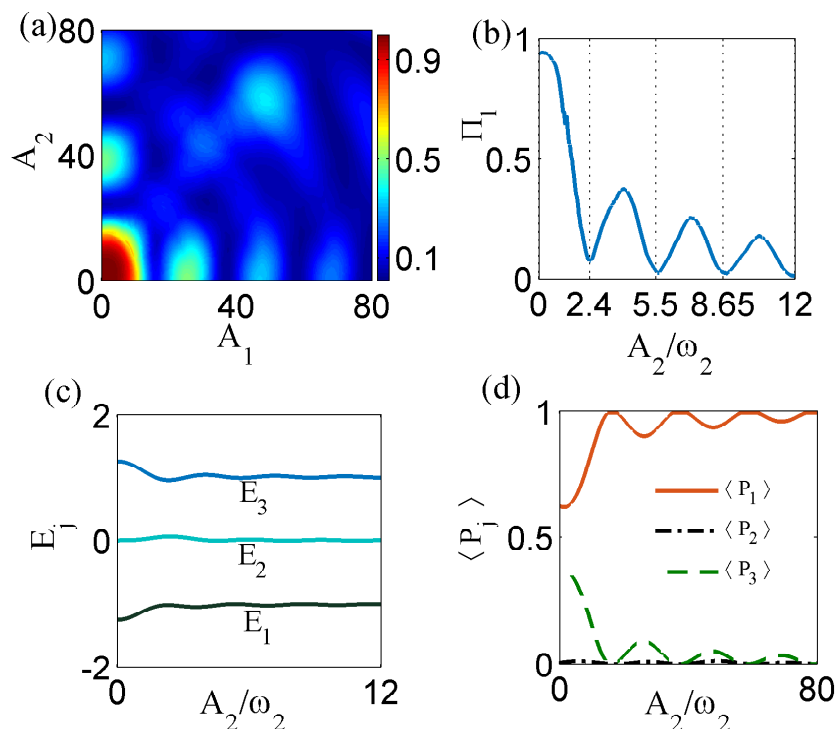


**Figure 6.** (Color online) (a) Evolution of  $\Pi_1$  as a function of  $A_1$  and  $A_2$  and such a 2/3rd  $\nu$ -photon resonance effect shows a clear dependence on driving amplitudes. (b) Evolution of  $\Pi_1$  versus  $A_2/\omega_2$  for  $A_1 = 10$ . The minimum values of  $\Pi_1$  are coincide with zeros of  $J_0(A_2/\omega_2)$ . (c) Quasienergies  $E_j$  versus  $A_2/\omega_2$  and (d) Time-averaged population  $\langle P_j \rangle$  corresponding to the medium quasienergies  $E_2$ . Other parameters are chosen as  $\omega_1 = 10$ ,  $\omega_2 = 20/3$  and  $\phi = 0$ .

We further reveal the dependence of resonance dynamics on driving amplitudes by a peculiar condition for  $A_1 = 10$  in Figure 6b. With the increase of  $A_2/\omega_2$ ,  $\Pi_1$  first experiences a transition from tunneling to almost complete suppression at  $J_0(A_2/\omega_2) = 0$  and then oscillates with a lower amplitude, implying partial tunneling suppression. The minimum values of  $\Pi_1$  are well consistent with zeros of  $J_0(A_2/\omega_2)$  due to the decoupling effect. So, particle’s transfer between three states can be adjusted with appropriate driving amplitudes even if at fractional- $\nu$ -th-order resonances.

Here, due to  $\omega_1 = 10$ ,  $\omega_2 = 20/3$ , Floquet theory works well for a common frequency  $\omega = \omega_1/3 = \omega_2/2$ . Quasienergy spectrum as a function of  $A_2/\omega_2$  is plotted in Figure 6c in which  $E_1$  and  $E_3$  are weakly influenced by varying amplitude  $A_2$  in the absence of avoided crossings or degeneracy. Based on the significant dependence of  $\Pi_1$  on driving amplitudes, we further check their eigenstates and find that the property of Floquet state corresponding to quasi-zero energy level  $E_2$  is consistent with  $\Pi_1$ , as shown in Figure 6d (The other two Floquet states with no localized states are not listed here). Therefore, we can see that driving amplitudes dependence is attributed to the modulated localized Floquet state.

#### 4.4. Dependence on Phase Differences

In the above discussion, we have not considered the roles played by the phase difference. In fact,  $\phi$  is useful in realizing quantum control if applied appropriately. Focusing on the 2/3rd-order resonance ( $\omega_1 = 10$ ,  $\omega_2 = 20/3$ ) again, Figure 7a shows tunneling probability  $\Pi_1$  with varying  $\phi$  and  $A_2$  for a driving amplitudes  $A_1 = 24$ . Significant influence of  $\phi$  is observed in the parameter region  $20 < A_2 < 40$ . So, tunneling probability can be enhanced by more than 0.5 by choosing appropriate values of  $\phi$  and  $A_2$ . Therefore,

the phase difference can have a large contribution to improving or suppressing tunneling probability.

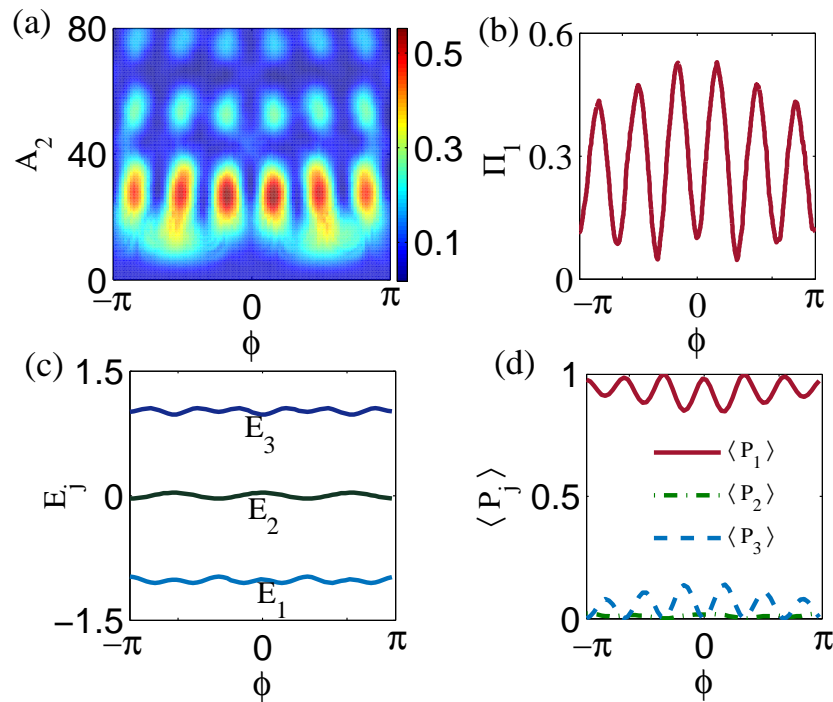


**Figure 7.** (Color online) (a) Evolution of  $\Pi_1$  as a function of  $\phi$  and  $A_2$  for  $A_1 = 24$ . (b–d) Tunneling probability  $\Pi_1$ , quasienergies and localized dark Floquet states versus the phase difference  $\phi$  varying from  $-\pi$  to  $\pi$ . Other parameters are the same as in Figure 6.

To establish a connection between phase dependence and Floquet properties, we plot  $\Pi_1$  as a function of  $\phi$  in Figure 7b under the condition of  $A_1 = 24$  which satisfies  $J_0(A_1/\omega_1) = 0$ . It is found that as  $\phi$  varies from  $-\pi$  to  $\pi$ , tunneling probability  $\Pi_1$  can be enhanced  $\sim 0.5$ . Also, the quasienergy spectra, as shown in Figure 7c, display that  $E_1$ ,  $E_2$  and  $E_3$  are all changed by the phase and the medium one  $E_2$  slightly oscillates around zero. Further study on the Floquet states, plotted in Figure 7d reveals that the phase dependence on  $\Pi_1$  is originated from the localized Floquet state corresponding to  $E_2$  with a negligible population at  $\langle P_2 \rangle$ . The other two Floquet states with no localized states are not shown here. Therefore, it is also the modulated dark Floquet state that leads to the change of tunneling probabilities.

### 5. Conclusions

In conclusion, we have presented a comprehensive analysis of resonance dynamics in a three-well system under two-frequency driving. We have explored two quantum effects including integer and fractional photon resonance utilizing standard Floquet theory and SFT method [37,42]. It is found that photon-assisted tunneling originates from the avoided crossing of Floquet spectra and has an intrinsic connection with the hybridization between different states at those resonance points. Moreover, our study on the two-frequency driving scheme further reveals that fractional resonances like the 2/3rd order can be triggered by tunneling dynamics. The numerical results agree well with analytical ones derived from the high-frequency approximation and demonstrate the effectiveness of Floquet theory for studying multiple frequency driving cases. Further studies on the driving amplitude and phase dependence provide a way to coherently enhance or suppress interwell tunneling. Our study can be extended to other odd- $N$ -state ( $N > 3$ ) systems with multi-frequency driving fields to probe even exotic resonance dynamics.

**Author Contributions:** Writing—original draft preparation, L.L.; writing—review and editing, W.L.; methodology, B.W. All authors have read and agreed to the published version of the manuscript.

**Funding:** The authors acknowledge the financial support from the National Natural Science Foundation of China (Grant No.12005319) and Team Research Project by Zhongyuan University of Technology (K2021TD006).

**Conflicts of Interest:** The authors declare no conflict of interest.

## References

1. Wu, Y.; Côté, R. Bistability and quantum fluctuations in coherent photoassociation of a Bose-Einstein condensate. *Phys. Rev. A* **2002**, *65*, 053603.
2. Longhi, S. Adiabatic quantum state transfer in tight-binding chains using periodic driving fields. *EPL* **2014**, *107*, 50003.
3. Anderson, P.W. Absence of diffusion in certain random lattices. *Phys. Rev.* **1958**, *109*, 1492.
4. Yin, T.-S.; Lü, X.-Y.; Zheng, L.-L.; Wang, M.; Li, S.; Wu, Y. Nonlinear effects in modulated quantum optomechanics. *Phys. Rev. A* **2017**, *95*, 053861.
5. Mallavarapu, S.K.; Niranjana, A.; Li, W.; Wuster, S.; Nath, R. Population trapping in a pair of periodically driven Rydberg atoms. *Phys. Rev. A* **2021**, *103*, 023335.
6. Xue, M.; Yin, S.; You, L. Universal driven critical dynamics across a quantum phase transition in ferromagnetic spinor atomic Bose-Einstein condensates. *Phys. Rev. A* **2018**, *98*, 013619.
7. Lü, X.-Y.; Jing, H.; Ma, J.-Y.; Wu, Y. PT-Symmetry-Breaking Chaos in Optomechanics. *Phys. Rev. Lett.* **2015**, *114*, 253601.
8. Zheng, S.B. Geometric phase for a driven quantum field subject to decoherence. *Phys. Rev. A* **2015**, *91*, 052117.
9. Luo, X.; Zeng, Z.-Y.; Guo, Y.; Yang, B.; Xiao, J.; Li, L.; Kong, C.; Chen, A.-X. Controlling directed atomic motion and second-order tunneling of a spin-orbit-coupled atom in optical lattices. *Phys. Rev. A* **2021**, *103*, 043315.
10. Hu, C.S.; Liu, Z.Q.; Liu, Y.; Shen, L.T.; Wu, H.; Zheng, S.B. Entanglement beating in a cavity optomechanical system under two-field driving. *Phys. Rev. A* **2020**, *101*, 033810.
11. Yang, W.L.; Song, W.L.; An, J.-H.; Feng, M.; Suter, D.; Du, J. Floquet engineering to entanglement protection of distant nitrogen vacancy centers. *New J. Phys.* **2019**, *21*, 013007.
12. Niranjana, A.; Li, W.; Nath, R. Landau-Zener transitions and adiabatic impulse approximation in an array of two Rydberg atoms with time-dependent detuning. *Phys. Rev. A* **2020**, *101*, 063415.
13. DeSalvo, B.J.; Patel, K.; Johansen, J.; Chin, C. Observation of a degenerate Fermi gas trapped by a Bose-Einstein condensate. *Phys. Rev. Lett.* **2017**, *119*, 233401.
14. Vretenar, M.; Kassenberg, B.; Bissesar, S.; Toebes, C.; Klaers, J. Controllable Josephson junction for photon Bose-Einstein condensates. *Phys. Rev. Res.* **2021**, *3*, 023167.
15. Luo, X.; Hu, Z.; Zeng, Z.-Y.; Luo, Y.; Yang, B.; Xiao, J.; Li, L.; Chen, A.-X. Analytical results for the superflow of spin-orbit-coupled Bose-Einstein condensates in optical lattices. *Phys. Rev. A* **2021**, *103*, 063324.
16. Wang, Y.; Gao, J.; Pang, X.-L.; Jiao, Z.-Q.; Tang, H.; Chen, Y.; Qiao, L.-F.; Gao, Z.-W.; Dou, J.-P.; Yang, A.-L.; Jin, X.-M. Parity-Induced Thermalization Gap in Disordered Ring Lattices. *Phys. Rev. Lett.* **2019**, *122*, 013903.
17. Li, L.-P.; Zhang, X.; Li, L.; He, Q.; Zheng, L.; Fu, S.; Liu, B. Loss-induced localization in a periodically driven nonlinear system. *Phys. Rev. A* **2019**, *100*, 033808.
18. Taya, H.; Hongo, M.; Ikeda, T.N. Analytical WKB theory for high-harmonic generation and its application to massive Dirac electrons. *Phys. Rev. B* **2021**, *104*, L140305.
19. Bairey, E.; Refael, G.; Lindner, N.H. Driving induced many-body localization. *Phys. Rev. B* **2017**, *96*, 020201(R).
20. Grossmann, F.; Dittrich, T.; Jung, P.; Hänggi, P. Coherent destruction of tunneling. *Phys. Rev. Lett.* **1991**, *67*, 516.
21. Kierig, E.; Schnorrberger, U.; Schietinger, A.; Tomkovic, J.; Oberthaler, M.K. Single-Particle Tunneling in Strongly Driven Double-Well Potentials. *Phys. Rev. Lett.* **2008**, *100*, 190405.
22. Xie, Q.; Rong, S.; Zhong, H.; Lu, G.; Hai, W. Photon-assisted tunneling of a driven two-mode Bose-Einstein condensate. *Phys. Rev. A* **2010**, *82*, 023616.
23. Betancur-Ocampo, Y.; Majari, P.; Espitia, D.; Leyvraz, F.; Stegmann, T. Anomalous Floquet tunneling in uniaxially strained graphene. *Phys. Rev. B* **2021**, *103*, 155433.
24. Biswas, R.; Sinha, C. Photon induced tunneling of electron through a graphene electrostatic barrier. *J. Appl. Phys.* **2013**, *114*, 183706.
25. Zeb, M.A.; Sabeeh, K.; Tahir, M. Chiral tunneling through a time-periodic potential in monolayer graphene. *Phys. Rev. B* **2008**, *78*, 165420.
26. Li, W.; Reichl, L.E. Floquet scattering through a time-periodic potential. *Phys. Rev. B* **1999**, *60*, 15732.
27. Yampol'skii, V.A.; Savel'ev, S.; Nori, F. Voltage-driven quantum oscillations in graphene. *New J. Phys.* **2008**, *10*, 053024.
28. Sias, C.; Lignier, H.; Singh, Y.P.; Zenesini, A.; Ciampini, D.; Morsch, O.; Arimondo, E. Observation of photon-assisted tunneling in optical lattices. *Phys. Rev. Lett.* **2008**, *100*, 040404.
29. Forster, F.; Muhlbacher, M.; Blattmann, R.; Schuh, D.; Wegscheider, W.; Ludwig, S.; Kohler, S. Landau-Zener interference at bichromatic driving. *Phys. Rev. B* **2015**, *92*, 245422.

30. Ding, Y.; Umbanhowar, P. Enhanced Faraday pattern stability with three-frequency driving. *Phys. Rev. E* **2006**, *73*, 046305.
31. Gambetta, F.M.; Zhang, C.; Hennrich, M.; Lesanovsky, I.; Li, W. Exploring the many-body dynamics near a conical intersection with trapped Rydberg ions. *Phys. Rev. Lett.* **2021**, *126*, 233404.
32. Teichmann, N.; Esmann, M.; Weiss, C. Fractional photon-assisted tunneling for Bose-Einstein condensates in a double well. *Phys. Rev. A* **2009**, *79*, 063620.
33. Esmann, M.; Teichmann, N.; Weiss, C. Fractional-photon-assisted tunneling in an optical superlattice: Large contribution to particle transfer. *Phys. Rev. A* **2011**, *83*, 063634.
34. Li, L.; Luo, X.; Yang, X.; Wang, M.; Lü, X.; Wu, Y. An analog of photon-assisted tunneling in a periodically modulated waveguide array. *Sci. Rep.* **2016**, *6*, 35744.
35. Lu, G.; Hai, W. Quantum tunneling switch in a planar four-well system. *Phys. Rev. A* **2011**, *83*, 053424.
36. Salger, T.; Kling, S.; King, T.; Geckeler, C.; Molina, L.M.; Weitz, M. Directed transport of atoms in a Hamiltonian quantum ratchet. *Science* **2009**, *326*, 1241.
37. Shirley, J.H. Solution of the Schrödinger Equation with a Hamiltonian Periodic in Time. *Phys. Rev.* **1965**, *138*, B979.
38. Zhang, Y.; Chen, Z.; Wu, B.; Busch, T.; Konotop, V.V. Asymmetric Loop Spectra and Unbroken Phase Protection due to Nonlinearities in  $\mathcal{PT}$ -Symmetric Periodic Potentials. *Phys. Rev. Lett.* **2021**, *127*, 034101.
39. Ho, T.-S.; Chu, S.-I.; Tietz, J.V. Semiclassical many-mode Floquet theory. *Chem. Phys. Lett.* **1983**, *96*, 464.
40. Booth, D.W.; Isaacs, J.; Saffman, M. Reducing the sensitivity of Rydberg atoms to dc electric fields using two-frequency ac field dressing. *Phys. Rev. A* **2018**, *97*, 012515.
41. Holthaus, M. Floquet engineering with quasienergy bands of periodically driven optical lattices. *J. Phys. B At. Mol. Opt. Phys.* **2016**, *49*, 013001.
42. Poertner, A.N.; Martin, J.D.D. Validity of many-mode Floquet theory with commensurate frequencies. *Phys. Rev. A* **2020**, *101*, 032116.
43. Grynberg, G.; Robilliard, C. Cold atoms in dissipative optical lattices. *Phys. Rep.* **2001**, *355*, 335.
44. Hemmerich, A. Effective time-independent description of optical lattices with periodic driving. *Phys. Rev. A* **2010**, *81*, 063626.
45. Görg, F.; Sandholzer, K.; Minguzzi, J.; Desbuquois, R.; Messer, M.; Esslinger, T. Realization of density-dependent Peierls phases to engineer quantized gauge fields coupled to ultracold matter. *Nat. Phys.* **2019**, *15*, 1161–1167.
46. Szameit, A.; Burghoff, J.; Pertsch, T.; Nolte, S.; Tünnermann, A.; Lederer, F. Two-dimensional soliton in cubic fs laser written waveguide arrays in fused silica. *Opt. Express* **2006**, *14*, 6055.
47. Longhi, S. Quantum-optical analogies using photonic structures. *Laser Photon. Rev.* **2009**, *3*, 243.
48. Longhi, S.; Marangoni, M.; Lobino, M.; Ramponi, R.; Laporta, P.; Cianci, E.; Foglietti, V. Observation of dynamic localization in periodically curved waveguide arrays. *Phys. Rev. Lett.* **2006**, *96*, 243901.
49. Szameit, A.; Kartashov, Y.V.; Dreisow, F.; Heinrich, M.; Pertsch, T.; Nolte, S.; Tünnermann, A.; Vysloukh, V.A.; Lederer, F.; Torner, L. Inhibition of light tunneling in waveguide arrays. *Phys. Rev. Lett.* **2009**, *102*, 153901.
50. Wu, B.; Niu, Q. Nonlinear Landau-Zener tunneling. *Phys. Rev. A* **2000**, *61*, 023402.
51. Li, L.; Wang, B.; Lü, X.-Y.; Wu, Y. Chaos-related localization in modulated lattice array. *Ann. Phys.* **2018**, *530*, 1700218.
52. Lignier, H.; Sias, C.; Ciampini, D.; Singh, Y.; Zenesini, A.; Morsch, O.; Arimondo, E. Dynamical control of matter-wave tunneling in periodic potentials. *Phys. Rev. Lett.* **2007**, *99*, 220403.
53. Holthaus, M. Towards coherent control of a Bose-Einstein condensate in a double well. *Phys. Rev. A* **2001**, *64*, 011601.
54. Novičenko, V.; Anisimovas, E.; Juzeliūnas, G. Floquet analysis of a quantum system with modulated periodic driving. *Phys. Rev. A* **2017**, *95*, 023615.
55. Rahav, S.; Gilary, I.; Fishman, S. Effective Hamiltonians for periodically driven systems. *Phys. Rev. A* **2003**, *68*, 013820.
56. Kennes, D.M.; Torre, A.d.; Ron, A.; Hsieh, D.; Millis, A.J. Floquet Engineering in Quantum Chains. *Phys. Rev. Lett.* **2018**, *120*, 127601.
57. Mikami, T.; Kitamura, S.; Yasuda, K.; Tsuji, N.; Oka, T.; Aoki, H. Brillouin-Wigner theory for high-frequency expansion in periodically driven systems: Application to Floquet topological insulators. *Phys. Rev. B* **2016**, *93*, 144307.
58. Lu, G.; Hai, W.; Zhong, H. Quantum control in a double well with symmetric or asymmetric driving. *Phys. Rev. A* **2009**, *80*, 013411.
59. Luo, X.; Li, L.; You, L.; Wu, B. Coherent destruction of tunneling and dark Floquet state. *New J. Phys.* **2014**, *16*, 013007.
60. Li, L.; Luo, X.; Lü, X.-Y.; Yang, X.; Wu, Y. Coherent destruction of tunneling in a lattice array with a controllable boundary. *Phys. Rev. A* **2015**, *91*, 063804.